water

MDPI

Article

Shrinkage Characteristics and Microstructure Evolution of Yili Loess under Different Wetting and Drying Cycles

Aynur Abduhell [1], Zizhao Zhang [1,2,*], Wenyu Cheng [1] and Yanyang Zhang [1]

[1] College of Geology and Mining Engineering, Xinjiang University, Urumqi 830017, China; aynur15894603133@163.com (A.A.); cwy606021@163.com (W.C.); zyy@xju.edu.cn (Y.Z.)
[2] State Key Laboratory for Geomechanics and Deep Underground Engineering, Xinjiang University, Urumqi 830017, China
* Correspondence: zhangzizhao@xju.edu.cn; Tel.: +86-13639977295

Abstract: The loess in Yili Valley is prone to landslides in the rainy season. We studied the influence law of shrinkage and the microstructure of the loess in Yili Valley under different wetting and drying cycles. Considering the climatic conditions and sampling depth of the study area, shrinkage tests were carried out under six kinds of dry and wet cycling paths. The fracture changes and shrinkage characteristics of the loess under different dry–wet cycling times were analyzed, and the deformation characteristics of the loess during the process of water-loss shrinkage under the dry–wet cycling conditions were discussed. The results show that (1) there is an exponential relationship between the number of dry and wet cycles and the final shrinkage rate. The influence of dry and wet cycles on the final shrinkage rate is significant in the early stage. (2) With the increase in the number of dry and wet cycles, the decline in the final shrinkage rate decreases, and the final shrinkage rate and shrinkage coefficient of soil also show a decreasing trend, while the soil sample area first increases and then gradually decreases, and the surface shrinkage cracking is gradually stable. The surface porosity tends to increase. (3) Under the action of repeated wet expansion and dry contraction, irregular cracks are produced inside the soil body, which leads to the increase in soil permeability, reduces the strength of the soil body, reflects the phenomenon of strength deterioration, and thus indicates the stability of loess slopes. The research results of this paper can provide an important parameter basis for the prevention and control of loess landslide geological disasters in Yili Valley.

Keywords: wet and dry cycle; Yili Valley; loess; shrinkage characteristics; image processing

Citation: Abduhell, A.; Zhang, Z.; Cheng, W.; Zhang, Y. Shrinkage Characteristics and Microstructure Evolution of Yili Loess under Different Wetting and Drying Cycles. *Water* **2023**, *15*, 2932. https://doi.org/10.3390/w15162932

Academic Editors: Changhyun Jun, Wooyoung Na and Sang Yeob Kim

Received: 12 July 2023
Revised: 6 August 2023
Accepted: 8 August 2023
Published: 14 August 2023

1. Introduction

Loess is a Quaternary wind-blown deposit that covers large arid and semi-arid regions at mid-latitudes across the globe. Loess fabric is mainly composed of skeleton particles or aggregates, which are dominated by clay, silt, sand, and soluble salt. The material composition, particle morphology, contact, and connection modes of loess are very complex. In dry conditions, a cemented structure system with certain strength is formed, and it easily loses its initial structural state when affected by humidification. This significantly affects the properties and quality of the soil, the productivity of the ecosystem, and the sustainability of environmental management, which leads to the failure of some large-scale constructions, the occurrence of natural disasters, and even the evolution of the global soil layer. For example, the frequent occurrence of loess landslides in Yili Valley of Xinjiang has seriously affected the normal production and life of human beings in this region. It is necessary to study the occurrence mechanism and influencing factors of landslides in this region. Yili region is widely distributed loess, loess has a wet subsidence, so in the drying process the volume occurs obvious contraction. During the drying process, the volume of loess shrinks, accompanied by soil cracking. During the humidification process, the volume expands obviously, and the strength and stiffness decrease significantly. Moreover, the loess

properties change after repeated dry–wet cycles for many years [1]. The characteristics of loess in this area play an important role in landslides. According to the Geological Environment Monitoring Institute of Yili Prefecture, 339 geological disasters occurred in Yili Valley from 2005 to 2020, of which 233 were landslides, accounting for 69% of the total. Multiple dry–wet cycles are among the important factors in loess landslides. Therefore, it is necessary to analyze the characteristics of loess in the study area.

Water is necessary for cement hydration and is also associated with the deterioration of most loess properties. Water can be used as the carrier of external erosion medium in loess, and it can also cause some deterioration of loess. The external environment that causes dramatic changes in the internal moisture of loess is the most typical and is commonly referred to as the dry–wet cycle environment. Because of this, the environment in which loess structures are subject to dry–wet cycles is usually considered to be the most typical, the harshest, and the most likely to cause loess durability problems [2–4]. Tse E et al.'s previous studies have shown that the dry–wet cycle is the controlling factor, and the dilatancy change characteristics are proposed through the shear strength test [5]. The influence of the soil–water characteristic curve of compacted silty soil was studied by observing initial dry density, water content, and stress state [6]. Some scholars agree that the tensile strength decreases significantly with the dry–wet cycle [7], the soil hydraulic conductivity increases gradually due to the dry–wet cycle [8], and the soil shrinks vertically [9]. The pore ratio of compacted loess increases gradually as the dry–wet cycle increases, and the dry density and cohesion decrease significantly [10]. Shao S J et al. found that the strength of collapsible loess decreases to the limit equilibrium state with the increase in water content to the critical water content ω_{cx} (the boundary point between the steady-rate drying stage and the slow-rate drying stage is called the critical point, and the corresponding average water content is the critical water content) during the dry–wet cycle [11], and the stress–strain equation of structural loess [12] was obtained. The dry–wet cycle will affect the soil deformation and strength characteristics [13]. There are significant differences in the influence of dry and wet cycling paths on the pores of unconfined and high-pressure bentonite aggregates [14]. Pires et al. agree that different frequencies of wet and dry cycles are related to the microstructure of loess [15,16]. Liu Ping et al. agree that soil deformation and cracking are related to soil shrinkage [17]. Wang Donglin et al. agree that shrinkage deformation occurs gradually with the decrease in soil saturation [18–20].

At present, most studies take the number of dry–wet cycles as the variable to analyze the deterioration law of the mechanical properties of loess. However, Ye, W. M. et al. reported that the attenuation of loess strength is not related to the development of soil swelling and shrinking cracks, and the crack evolution law also lacks a quantitative description. Some scholars have proposed reasonable recommended thresholds and magnification times in SEM tests [21], and proposed soil SEM image optimization processing technology to change binarization and parameter analysis content [22]. Moreover, a 3D analysis module of GIS has been used to realize a 3D display of the surface fluctuation state of soil sample particles [23]. Using a videolab image analysis system, a quantitative evaluation of the type of microstructures was carried out [24–27], along with the preliminary classification of the microstructures of soils [28,29]. In fact, the development of cracks is the fundamental factor causing loess strength attenuation, and the dry–wet cycle directly promotes the development of cracks in loess, resulting in the rapid expansion and penetration of cracks [30–33]. Therefore, the development of cracks should be fully considered when determining the soil strength index. Crack shape parameters (such as crack length, area ratio, width, etc.), which are closely related to soil engineering characteristics, are used as quantitative indexes to describe the degree of crack evolution. Tovey Smart and Krinsley et al. [34,35] combined existing image processing technology. Tang et al. [36–38] studied the influence of wetting and drying cycles on the morphological characteristics of the soil surface fracture network. The results showed that the moisture content of cracking, the surface fracture rate, and the thickness of completely dried soil increased significantly with the increase in the number of wetting and drying cycles. Vogel et al. [39] analyzed the dynamic process of soil surface

crack development by using image processing technology, summarized several fracture modes, and found that the frequency distribution of the fracture intersection angle was not significantly affected by the dry–wet cycle. Güllü H. et al. analyzed the proper replacements of the flow properties, and unconfined compressive strength (UCS) and ultrasonic pulse velocity (UPV) tests were performed to determine the strength quality (7-day, 28-day) of grout specimens [40]. Güllü H. et al. analyzed the rheology and strength performances of cement (PC)-based grouts with the stabilizers of limestone dust (LD), bottom ash (BA), geopolymerized cold-bonded limestone dust (GLD), and geopolymerized cold-bonded bottom ash (GBA) [41]. Güllü, H. et al. employed the dosages of stabilizers and the number of freeze–thaw cycles as input (predictor) variables and UCS as the output variable. To understand the dominant parameter of the predictor variables on the UCS of stabilized soil, a sensitivity analysis was performed. The performance measures of root mean square error (RMSE), mean absolute error (MAE), and determination coefficient (R2) were used to evaluate the prediction accuracy and applicability of the employed models. The results indicate that the predictions, based on the AI techniques employed, are significantly correlated with the measured UCS [42].

Previous research results mainly used soil structure, permeability coefficient, density, and strength as single or multiple factors to study loess characteristics. The repeated alternations in rainfall and evaporation are among the important reasons for the occurrence of landslides, and the dry–wet cycle deterioration of loess also has a great influence on landslides [43]. Therefore, it is necessary to study the deterioration effects of the strength and microstructure of remodeled loess under different initial moisture contents and dry–wet cycles. Based on the influence of different initial moisture contents and the number of dry–wet cycles on loess characteristics, we conducted dry–wet cycle experiments on Yili Valley loess by the laboratory test method and analyzed the influence law of water-holding characteristics and shrinkage characteristics of loess. This work provides some theoretical guidance for regional geological disaster prevention.

2. Materials and Methods

2.1. Overview of the Study Area

The study area is Xinyuan County, Ili Kazakh Autonomous Prefecture, Xinjiang Uygur Autonomous Region, China, which is located at the eastern end of the Ili River Valley in western Xinjiang, surrounded by mountains to the south, east, and north and open in the west, with an overall high terrain in the east and low in the west, high on both sides and low in the middle, and with topography dominated by mountains, hills, and river valley plains. The study area belongs to the northern temperate semi-arid continental climate zone, with four distinct seasons, abundant precipitation, sufficient sunshine, and abundant light and heat resources. The rock body in the study area is mainly hard massive rock groups, mainly distributed on the south side of the mountain pass in the study area. Under the silty soil layer, the distribution is not continuous, the thickness is not uniform, and the lithology is light flesh red gray-white monoclinic granite and gray-white fine-grained porphyritic monoclinic granite.

2.2. Test Materials

The loess samples were taken from Xinyuan County, Yili Region, Xinjiang, China, with a depth of 0–2 m and a width of 2 m. The soil samples were yellowish-brown. The coordinates of the study area are 43°25′05.17″ north latitude and 83°40′05.89″ east longitude, as shown in Figure 1.

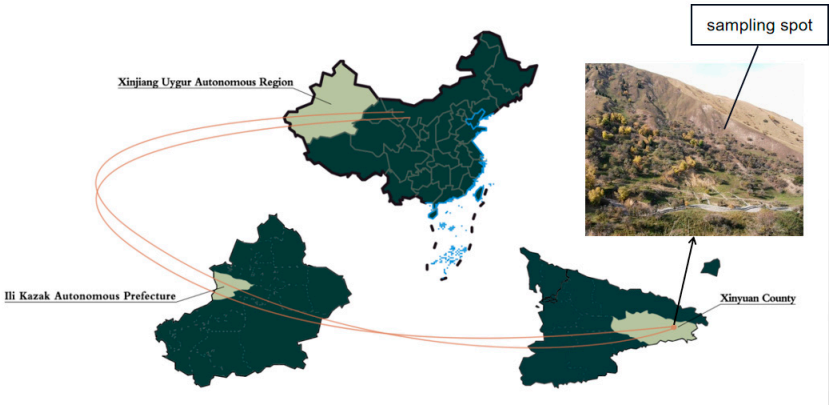

Figure 1. Location map of the study area.

In order to understand the basic properties of the soil samples and provide a parameter basis for the later remodeling of the samples, water content tests, density tests, particle analysis tests, and limit water content tests were carried out to obtain undisturbed soil samples with a penetration sampler, and the basic physical properties of some undisturbed soil samples were obtained, as shown in Table 1. The natural water content of the soil sample is 26.7%, the density is 1.72 g/cm^3, the dry density is 1.42 g/cm^3, the plastic limit is 18.34%, the liquid limit is 29.09%, the plastic index is 10.79, the liquid index is 0.75, and the maximum dry density is 1.86 g/cm^3.

Table 1. Basic physical properties of the undisturbed sample.

Physical Property Index	Natural Moisture Content (%)	Density (g/cm^3)	Dry Density (g/cm^3)	Plastic Limit (%)	Liquid Limit (%)	Plasticity Index	Liquid Index	Maximum Dry Density (g/cm^3)
Specimen	26.7	1.72	1.42	18.34	29.09	10.79	0.75	1.86

2.3. Sample Preparation

After the field sampling was completed, the sample was transported to the soil mechanics laboratory for indoor test analysis. The experiment in this study used a remodeled sample and set a parameter basis for the post-production of remodeled samples. The disturbed soil samples collected on-site were first air-dried and pre-treated in the laboratory. The air-dried soil samples were screened by 2 mm standard and stored in a sealed container for future use. According to the moisture content test, the moisture content of the air-dried samples was 2.05%. Then, 54 remodeled ring knife samples of loess with diameters of 61.8 mm and 20 mm were prepared for the dry and wet cycle test and the shrinkage test. As the saturated moisture content of the study area is 30% and the optimal moisture content is 20% under the condition of a rainstorm, the variation range of moisture content in the dry–wet cycle is designed to be 30–15%. In order to study the influence law of initial moisture content on loess in more detail, some samples are shown in Figure 2.

In order to facilitate the analysis and distinction of the influence of cyclic parameters, three initial moisture contents were set in the dry and wet cycle test: 30%, 25%, and 20%. By comparing the dry and wet cycle effects, the difference in the influence of initial moisture content and cyclic amplitude could be analyzed. According to relevant data, the optimal moisture content of loess in the reconstructed loess soil layer is 20%. Therefore, 20% was selected as the initial moisture content of one group of cyclic paths, 30% saturated moisture content of the soil sample was selected as the initial moisture content of the other group, and the natural moisture content is 26.7%, so 25% was chosen as the initial moisture content of the second path. The soil sample was slowly dried to the quality of the soil sample corresponding to the initial moisture content of each path. After preparation, the sample was stored in the moisturizing tank to maintain the original moisture content. According

to the above cyclic path setting principles, the three groups of dry and wet cyclic path parameters are shown in Table 2.

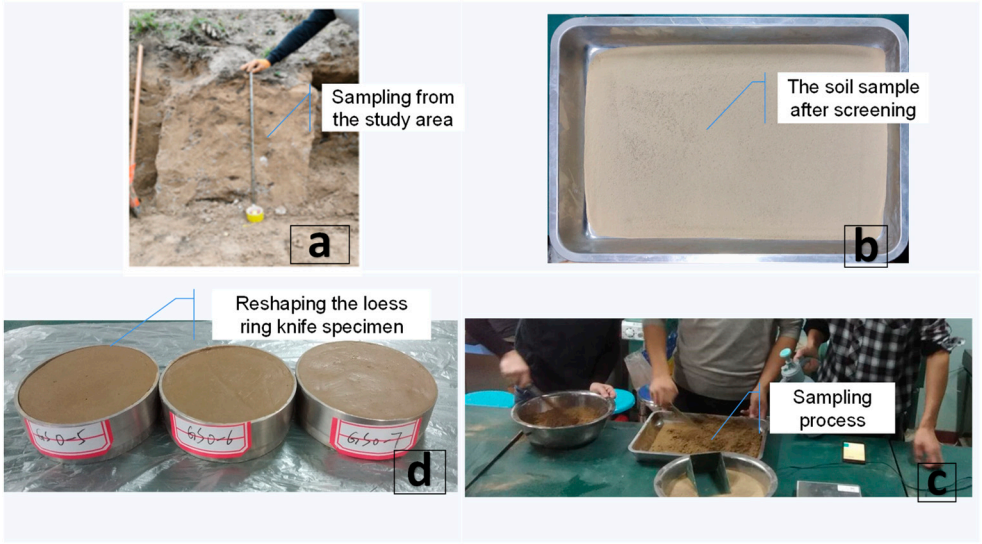

Figure 2. The sample preparation process of the specimen used in the test. (**a**) Sampling process in the study area at a depth of 2 m. Preparation of dry and wet cycle test; (**b**) sieved soil samples with particles up to 2 mm in size; (**c**) soil sample preparation process, preparation of post-test samples based on designed moisture content; (**d**) reshaping the loess ring knife sample.

Table 2. Parameter control table in the process of dry–wet cycle test.

Paths	Starting Moisture Content/%	Lower Limit Moisture Content/%	Range	Number of Times
Path 1	30%	15%	5	9
Path 2	25%	15%	5	9
Path 3	20%	15%	5	9

1. Preparation of shrinkage test

During the drying process, the volume of loess shrinks obviously, accompanied by soil cracking, while during the humidification process, the volume expands significantly, and the strength decreases significantly. Therefore, the shrinkage experiment was designed to observe the change in the shrinkage characteristic curve of loess samples before and after cyclic treatment.

According to the test methods of soils for highway engineering [44], after the dry–wet cycle test, the shrinkage test was started. In the shrinkage test, the dry–wet cycle process is first dry and then wet, and one cycle ends after each humidification. When preparing samples with 30%, 25%, and 20% moisture content, according to Formula (1), 273.89 g, 224.89 g, and 195.49 g of water, respectively, should be added per 1 kg of air-dried soil. In the shrinkage experiment, the volume of the ring knife was 59.96 cm^3. According to Formula (2), it was calculated that the masses of the soil samples with 30%, 25%, and 20% moisture content to be loaded into the ring knife were 110.69 g, 106.43 g, and 102.17 g, respectively.

$$m_w = \frac{m}{1 + 0.01 w_h} \times 0.01 \, (w - w_h) \quad (1)$$

where m_w is the soil sample requiring additional water (g), m is the mass of the soil sample for moisture content of dry air (g), w_h is the moisture content of air-dried soil (%), and w is the moisture content needed from the soil sample (%).

$$m = (1 + 0.01w)\rho_d V \quad (2)$$

where m is the mass of soil needed to prepare the disturbed soil sample (g), ρ_d is the dry density needed to prepare the soil samples (g/cm^3), and V is the volume of percussive or compacted soil measured (cm^3).

2. Preparation of microscopic test

The deformation characteristics of loess include swelling and shrinking deformation and cracking deformation. The formation of initial cracks provided powerful conditions for rainwater infiltration, which intensified the development of cracks and the swelling and shrinking of loess. Repeated wetting and drying cycles further developed cracks and the swelling and shrinking of loess, so the cracks and shrinkage in the dehumidification process of loess were analyzed to explain the anisotropy of loess shrinkage. The relationship between initial moisture content and the shrinkage direction of loess was studied.

After the shrinkage test, the microscopic test was carried out to test the change in fissure area and shrinkage area in the dehumidification process of different dry and wet cycles and the distribution of the width, length, and area indexes of complete dehumidification cracks, and the samples with 30%, 25%, and 20% moisture content were prepared. Three groups of tests were established with the same conditions for each test, and the three groups of tests were carried out at the same time.

2.4. Experimental Design

2.4.1. Wet and Dry Cycle Test Design

Based on the previous study, the change in samples was not evident after 9 dry and wet cycles. Thus, the maximum number of dry and wet cycles in this test was set at 9, and testing took place after 0, 1, 3, 5, 7, and 9 cycles.

1. Dehumidification

The sample dehumidification process followed the drying procedure, using an electric blow dryer to dehumidify, with the temperature set to 40 °C. Remove the humidified specimen from the moisture bottle for 24 h during drying, put the specimen in the drying oven, remove the specimen and weigh it hourly at an early stage, and weigh once every 10 min when the moisture content of the test reaches approximately 17% for drying to the specified moisture content of 15%.

2. Humidification

The humidification process of the sample was measured by the titration method, using an iron frame table and a burette humidifier, with the titration rate controlled at 0.05 mL/s. For samples with 30%, 25%, and 20% water content, according to Formula (3), the masses of the samples before humidifying were 110.69 g, 106.43 g, and 102.17 g. According to Formula (4), the water content after humidification is 30%, 25% and 20%, and the amount of water added to the specimen is 12.70 g, 8.52 g and 4.26 g. The samples were placed in a closed moisture reservoir for 24 h to provide uniform test infiltration, after which the sample humidification process was completed.

$$m = (1 + 0.01w_h) \cdot \rho_d v \quad (3)$$

where m is the total mass required for the preparation of soil samples (g). ρ_d is the dry density needed to prepare the soil sample (g/cm^3). v is the volume of compacted soil samples (cm^3). w_h is the air dry moisture (%).

$$m_w = \frac{m_0}{1 + 0.01w_h} \times 0.01(w - w_h) \quad (4)$$

where m_w is the amount of water to be added to the soil samples (g). m_0 is the mass of air-dried moisture-containing soil samples (g). w is the required humidity content of soil samples (%).

3. Dry and wet cycle process

Using a constant temperature and humidity test chamber to dry the specimen, the cycle process was first dry and then wet, and humidification occurred at the end of the cycle. The dry and wet cycle process is shown in Figure 3. In order to give full play to the deterioration effect of dry and wet cycling on the strength of loess, a dry and wet cycling path was set (see Table 3), and the dry and wet cycling test process is shown in Figure 4.

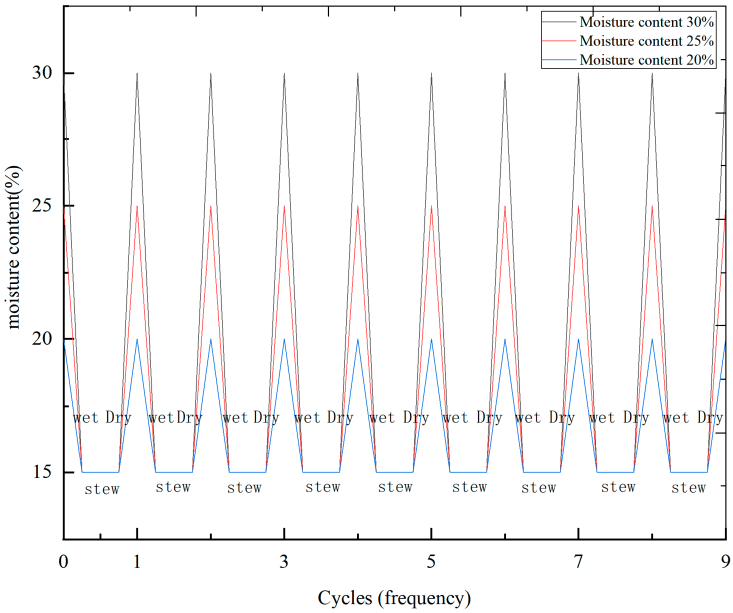

Figure 3. Illustration of drying–wetting cycle process.

Table 3. Dry and wet cycle scheme.

Soil Sample Number	Number of Samples	Initial Moisture Content	Dehumidification Path	Humidification Path	Cycles
0-1	3	30%	30–15%	15–30%	0
0-2	3	25%	25–15%	15–25%	0
0-3	3	15%	20–15%	15–20%	0
1-1	3	30%	30–15%	15–30%	1
1-2	3	25%	25–15%	15–25%	1
1-3	3	15%	20–15%	15–20%	1
3-1	3	30%	30–15%	15–30%	3
3-2	3	25%	25–15%	15–25%	3
3-3	3	15%	20–15%	15–20%	3
5-1	3	30%	30–15%	15–30%	5
5-2	3	25%	25–15%	15–25%	5
5-3	3	15%	20–15%	15–20%	5
7-1	3	30%	30–15%	15–30%	7
7-2	3	25%	25–15%	15–25%	7
7-3	3	15%	20–15%	15–20%	7
9-1	3	30%	30–15%	15–30%	9
9-2	3	25%	25–15%	15–25%	9
9-3	3	15%	20–15%	15–20%	9

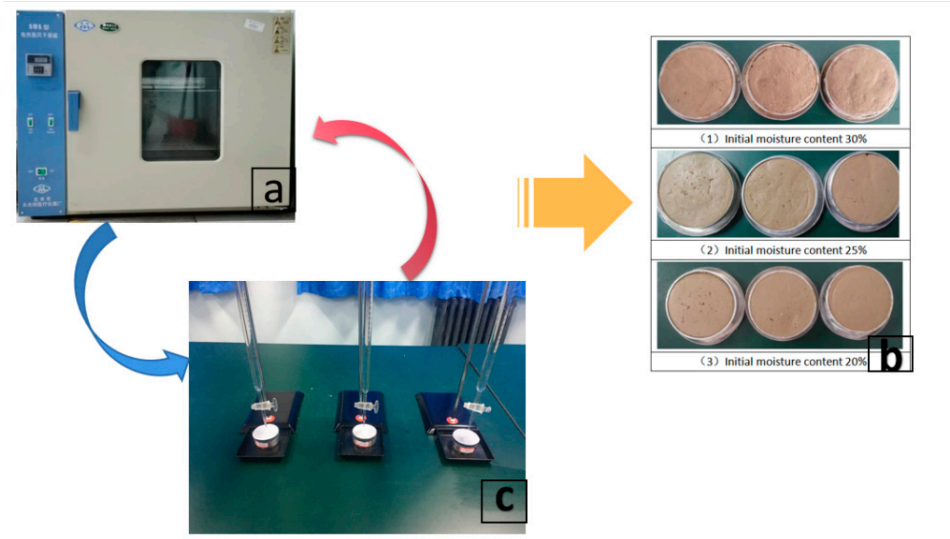

Figure 4. Wet and dry cycle test process. (**a**) Electric blast drying oven used for dehumidification, with temperature controlled at 40 °C for drying. (**b**) Sample humidification process using titration method, using an iron frame table and burette to form a humidification device, with titration rate controlled at 0.05 mL/s. (**c**) Samples with 30%, 25%, and 20% moisture content after dry and wet cycle tests, respectively.

2.4.2. Shrinkage Test Design

This experiment used the soil narrowing instrument SS-1 (see Figure 5). The narrowing test was divided into 6 groups depending on the number of dry and wet cycles, i.e., 0, 1, 3, 5, 7, and 9 cycles, taking samples of each moisture content from 3 specimens per group, for a total of 9 specimens, with two from each group selected to perform the shrinkage test. Next, we calculated and analyzed the shrinkage and deformation characteristics of water content and line shrinkage in the process of water loss and shrinkage according to Equation (5). To prevent the deformation of the test pieces in the process of increasing and decreasing humidity, two test pieces under each dry and wet cycle group for parallel tests were used.

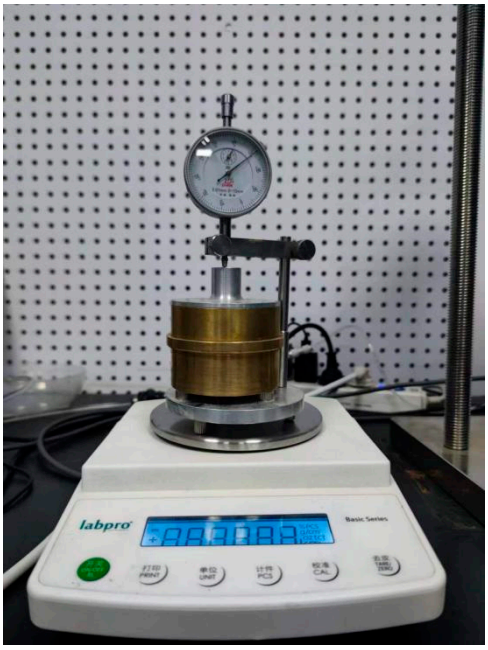

Figure 5. Observation meters of specimen shrinkage.

We calculated the line shrinkage rate according to the following formula:

$$e_{sL} = \frac{R_t - R_0}{H_0} \times 100 \quad (5)$$

where e_{sL} is linear withdrawal (%), calculated as 0.01. H_0 is the sample height (mm). R_0 is the initial reading of the measurement device as a percentage (mm). R_t is the percent reading of the counter (mm) at some point during the removal process.

2.4.3. Micro-Experimental Design

The study area experiences repeated dry and wet cycling of the side-slope loess due to seasonal alternations and temperature changes. This has a significant impact on loess microstructures and macrostructures and will lead to slope instability in severe cases. Therefore, the determination of the microstructure of the specimen was carried out, and Image-Pro Plus 6.0 software to perform binary processing (IPP, a digital image processing software, Version 6.0, Media Cybernetics, Inc., Rockville, MD, USA), image segmentation, and data statistics on the obtained electron microscope images was chosen in this study to observe changes in sample microstructures after three cyclic treatments. To identify the fracture network, the software can import different fracture images, and automatic binarization is performed. The software can automatically identify blocks in the fracture network, repair fracture segments, and remove impurity points. Moreover, it can identify the fracture network and statistical fracture geometry parameters, and display the resultant vector images.

Mu, Y. H. et al. also quantitatively assessed the fracture and interstitial space of loess by microscopically observing the fracture surface ratio and the surface porosity index [36], in which the ratio of the fracture surface is the ratio of the fracture surface to the original surface of the sample. Surface porosity is calculated as follows:

$$N = s_h / s_1 \quad (6)$$

where s_h is the total surface occupied by the pores (μm); s_1 is the total surface of the entire image (μm).

The total surface area of the pores can be computed by the software, and the total surface area of the entire image is known.

Qiang Tang et al. vectorized the images [45] and calculated the quantitative rupture and withdrawal parameters. After the binarization process, fractures of various lengths and widths were obtained, and the fracture zone of the sample and the zone of the surface pore area were obtained.

3. Results

Water is an important factor in the stability of loess slopes. During dry and wet cycles, the soil expands and contracts several times, and in this process, unstructured cracks are formed inside the soil. This series of cracks not only increases the permeability of the soil itself but also reduces the strength of the soil, which in turn modifies the technical characteristics of the loess slopes. The above tests measured the growth curves of relative expansion and contraction in loess under conditions of dry and wet cycles and different initial moisture levels. In order to better understand the change rule of permeability of loess under dry and wet cycles, parameters such as water content, line shrinkage, shrinkage coefficient, final line shrinkage, fissure area ratio, and area porosity were analyzed.

3.1. Variation Rules of Moisture Content with Time

Under different dry–wet cycles, the relation curve of moisture content with time is shown in Figure 6, from which it can be seen that the moisture content gradually decreases with the increase in time. When the initial moisture content is 30%, the decrease rate of moisture content is large between 0 and 16 h at the beginning of the test, and the curve

gradually slows down after 16 to 50 h and becomes stable after 50 h. When the initial water content is 25%, the decrease rate of water content is large between 0 and 25 h, and the curve gradually slows down after 25 to 60 h and becomes stable after 60 h. When the initial water content is 20%, the decrease rate of water content is large between 0 and 33 h, and the curve gradually slows down after 35 to 65 h and becomes stable after 65 h. In general, the curve shows a linear relationship. As can be seen from Figure 6, the overall moisture content presents a trend of first fast and then slow change. Under multiple dry–wet cycles, different initial moisture contents have the same trend of change. With the decrease in moisture content, pore water in soil samples is discharged continuously. It takes quite a long time to stabilize. This phenomenon shows that the deformation of loess is mainly concentrated in the early stage, and the deformation rate in the late stage is very small. The change in water content is the key reason for the shrinkage of soil. The loess is generally in an unsaturated state, and its moisture migrates downward in the form of unsaturated seepage or water vapor. Although the initial moisture content of the central loess is low and its water-holding capacity is also low, its water content changes little. Therefore, it can be concluded that water content is an important factor affecting the engineering properties of the loess. Both cohesion and internal friction angle decrease, which directly affects soil strength. The cement among the loess particles has very poor water resistance, which makes the loess very sensitive to the action of water. The migration of water in the soil makes the soil loose and weakens the bond between the soil particles.

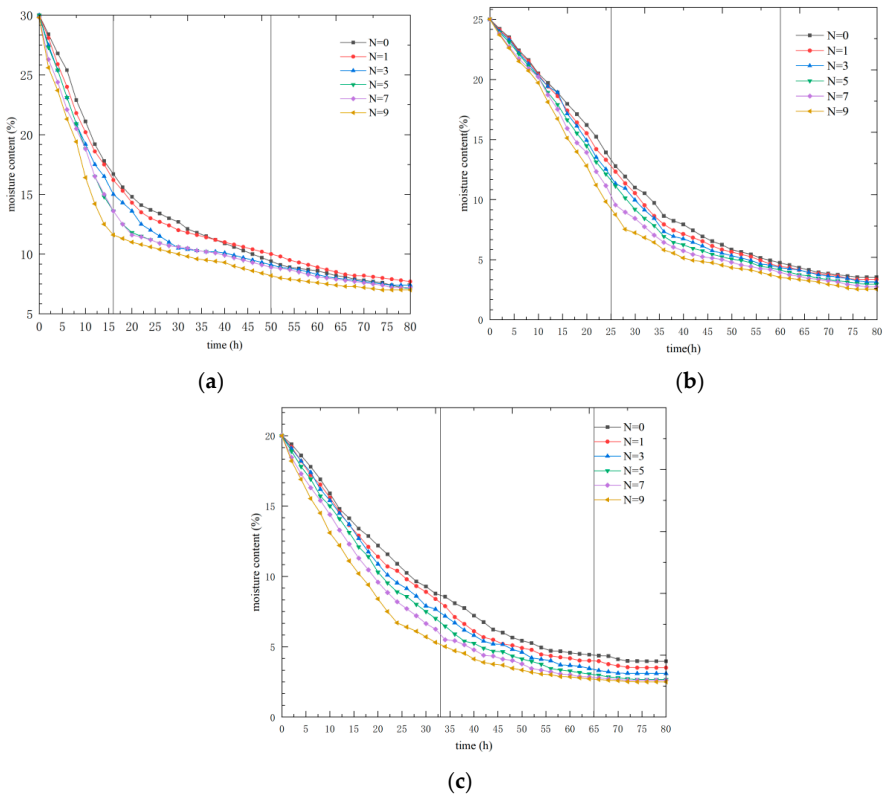

Figure 6. Water content–time relationship graph. (**a**) Curves of soil samples with an initial moisture content of 30% as a function of time under different wet and dry cycling conditions. (**b**) Curves of soil samples with an initial moisture content of 25% as a function of time under different wet and dry cycling conditions. (**c**) Curves of soil samples with an initial moisture content of 20% as a function of time under different wet and dry cycling conditions.

3.2. Properties of Water Loss and Shrinkage Curve in Dry and Wet Cycles

The characteristics of water loss and shrinkage of unsaturated loess were examined using unsaturated remodeled loess samples as an example, and we studied the law of

variation in the shrinkage rate of the study line with time and moisture content under a different number of cycles and different moisture content conditions.

3.2.1. Variation in Line Shrinkage Rate with Time

As shown in Figure 7, the rate of change in line shrinkage was high at the onset of the test, and the rate of line shrinkage increased over time. It showed a fast and slow change trend, with the same change trend for different initial moisture levels under several wet and dry cycles, and tended to remain stable following rapid water loss. When the initial moisture content is 30%, the rate of change is rapid to 0~15, and the rate of change in line narrowing decreases between 15 and 30 h and the curve becomes slow; after 30 h, the line-narrowing pattern tends to be stable. When the initial moisture content is 25%, the rate of change is rapid between 0 and 20 h, and the rate of variation in line narrowing decreases from 20 to 35 h and the curve becomes slow; after 35 h, the line shrinkage change becomes stable. When the initial moisture content is 20%, the rate of change is rapid between 0 and 25 h, and the rate of variation in line narrowing decreases after 25 h. The curve becomes slow and steady. The stability of the line narrowing is dependent on the number of cycles. The time of stabilization of the withdrawal rate of the line is also different, because the water in the interstitial space is continually dissipated. Soil particles are gradually collected, and the volume of soil mass steadily decreases. The height and diameter of the soil specimen are continually reduced over time. This means that the structure of the soil pores has a more visible shrinkage deformation, and eventually, the structure of the soil pores tends to be stable.

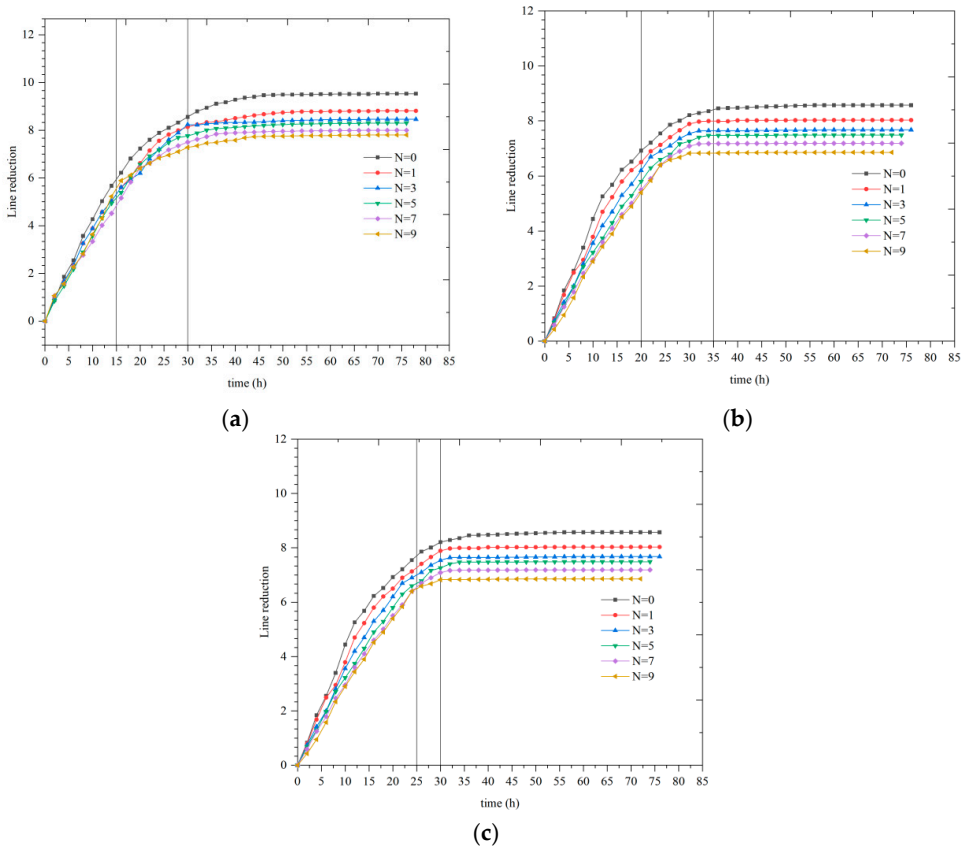

Figure 7. Plot of linear shrinkage versus time. (**a**) Curves of line shrinkage versus time for soil samples with an initial moisture content of 30% under different wet and dry cycling conditions. (**b**) Curves of line shrinkage versus time for soil samples with an initial moisture content of 25% under different wet and dry cycling conditions. (**c**) Curves of line shrinkage versus time for soil samples with an initial moisture content of 20% under different wet and dry cycling conditions.

3.2.2. Line Withdrawal Rate with Humidity Change Law

The withdrawal curve was obtained by the relationship between linear withdrawal and moisture content (see Figure 8). Figure 8 illustrates how the soil shrinkage process can be divided into three steps [45]: the linear withdrawal phase, the slope of which is the withdrawal coefficient; the deceleration phase; and the quasi-horizontal phase. In the linear withdrawal stage, as the water content decreases, the pore water in the soil sample is continually released. The extraction of the matrix is continually increased, the soil particles gradually collect, and the volume of the soil is continually contracted. This is expressed in the change in height of the sample as its linear shrinkage rate is continuously greater, and it is fundamentally linear with the change in its moisture content. In the withdrawal step, with the progressive reduction in the water content, the connection between the soil particles is closer, and at this point, the soil shrinkage caused by the reduction in water content is smaller and smaller, and the shrinkage is in the transitional phase. Near the horizontal phase, the connection of the soil particulate skeleton essentially tends to be stable, and with the change in soil internal stress caused by the reduction in moisture content, it is difficult to overcome the force of interaction between soil particles and cause movement. The ground does not shrink anymore and the rate of line narrowing does not change anymore, because the rate of line narrowing with the water content reaches some degree and gradually tends toward stabilization.

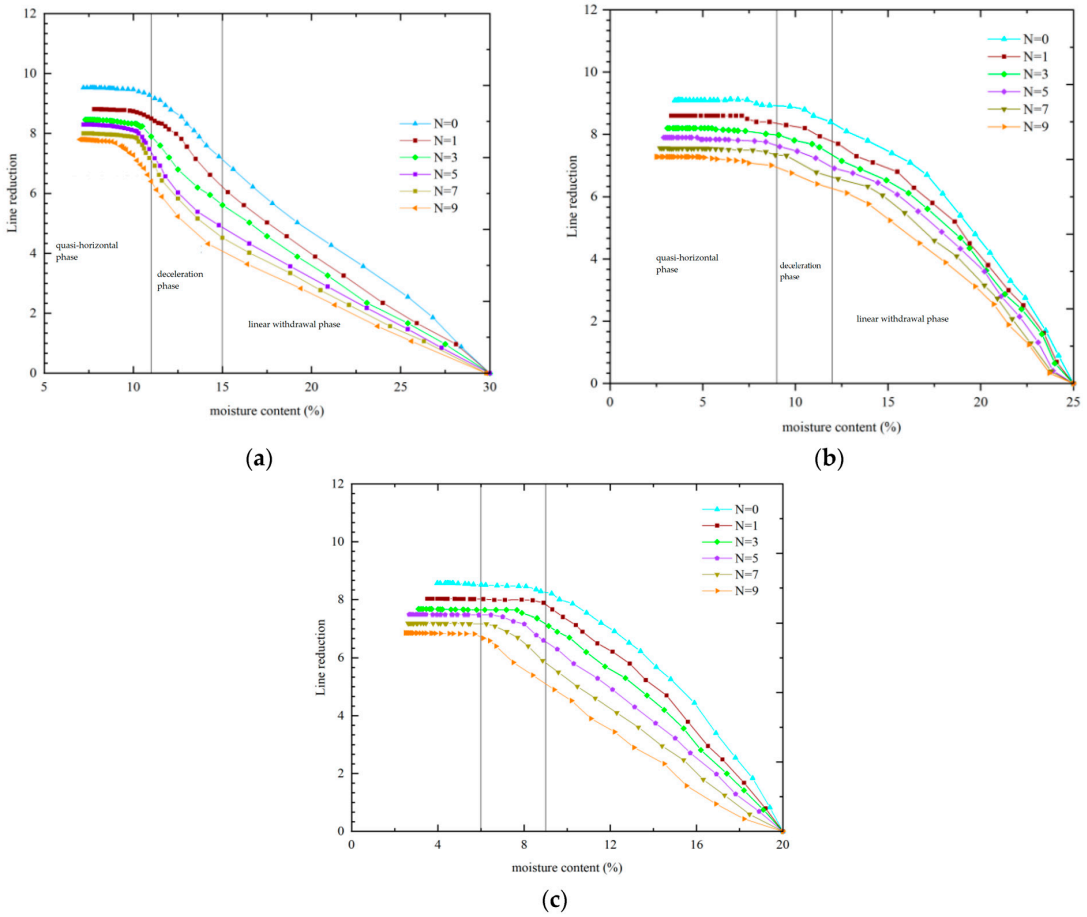

Figure 8. Shrinkage–water content relationship. (**a**) Curves of line shrinkage versus moisture content for soil samples with an initial moisture content of 30% under different wet and dry cycling conditions. (**b**) Curves of line shrinkage versus moisture content for soil samples with an initial moisture content of 25% under different wet and dry cycling conditions. (**c**) Curves of line shrinkage versus moisture content for soil samples with an initial moisture content of 20% under different wet and dry cycles.

3.3. Adjustment of the Shrinking Curve Equation in Dry and Wet Cycles

Six groups of specimens with original water contents of 30%, 25%, and 20% were compared and analyzed. Collins K, McGown A., et al. also analyzed the effect of loess water retention capacity under various initial water content conditions through shrinkage curves [45]. There were two identical parallel samples in each experimental group, and the average linear removal value of the parallel samples was taken for analysis. The results of the analysis are presented in Figure 9.

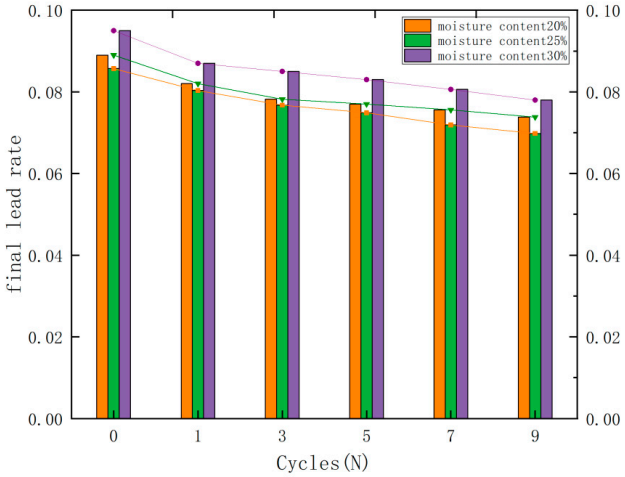

Figure 9. Final line shrinkage and number of cycles.

From Figure 9, we can see that the final line narrowing decreases with the increase in the number of wet and dry cycles [43]. The patterns of soil shrinkage curves for different numbers of wet and dry cycles are similar, and soil shrinkage curves under different cycling conditions can be adjusted. The equation of the regression curve of water content and shrinkage can be derived (see Table 4).

Table 4. Equation of soil shrinkage curve with different numbers of cycles.

Initial Moisture Content 30%		
Cycle Times	**Regression Equation**	**Correlation Coefficient**
0	$\delta = -1.1289\ w^2 - 0.0268\ w + 0.1062$	0.9922
1	$\delta = -0.6707\ w^2 - 0.1720\ w + 0.1092$	0.9898
3	$\delta = -0.4620\ w^2 - 0.2352\ w + 0.1083$	0.9848
5	$\delta = -0.1299\ w^2 - 0.3543\ w + 0.1140$	0.9842
7	$\delta = 0.0748\ w^2 - 0.4160\ w + 0.1143$	0.9857
9	$\delta = 0.1333\ w^2 - 0.4221\ w + 0.1103$	0.9881

Note: w is the water content of the sample; δ is the line shrinkage rate. (Because the contraction curve change law is similar for the water contents of 30%, 25%, and 20%, we mainly discuss the contraction curve changes for the water content of 30%.)

Based on the above calculations, we can see that the final shrinkage rate for samples under different cycle times is different, and the curve of the final line shrinkage ratio according to different cycle times is decreased (Figure 9). It is possible to observe that the final shrinkage rate of the samples is exponentially linked to the cycle times. The descriptive equations are shown in Equations (7)–(9).

$$\delta z = 0.0941 e^{0.064n} \quad (7)$$

$$\delta z = 0.0891 e^{-0.023n} \quad (8)$$

$$\delta z = 0.0836e^{-0.022n} \quad (9)$$

Equations (7)–(9) are equations for 30%, 25%, and 20% moisture content, respectively, where n is the number of wet and dry cycles, and δ is the rate of line narrowing. The correlation coefficients between the computed results and the experimental test results for 30%, 25%, and 20% moisture content are 0.987, 0.975, and 0.958, respectively.

3.4. Coefficient of Withdrawal of Loess under the Effect of Dry and Wet Cycles

Depending on the shrinkage curves of Yili loess for different numbers of wet and dry cycles, the effect of wet and dry cycles is known to significantly reduce loess. To estimate the response of shrinkage deformation to the change in moisture content, the soil shrinkage coefficient analysis was performed. The slope within the linear shrinkage phase is the soil specimen shrinkage coefficient, and a linear adjustment was made for this phase. As the number of wet and dry cycles increases, the slope becomes progressively smaller. The adjusted straight line is shown in Figure 10, and the adjusted equation and primary parameters are shown in Table 5.

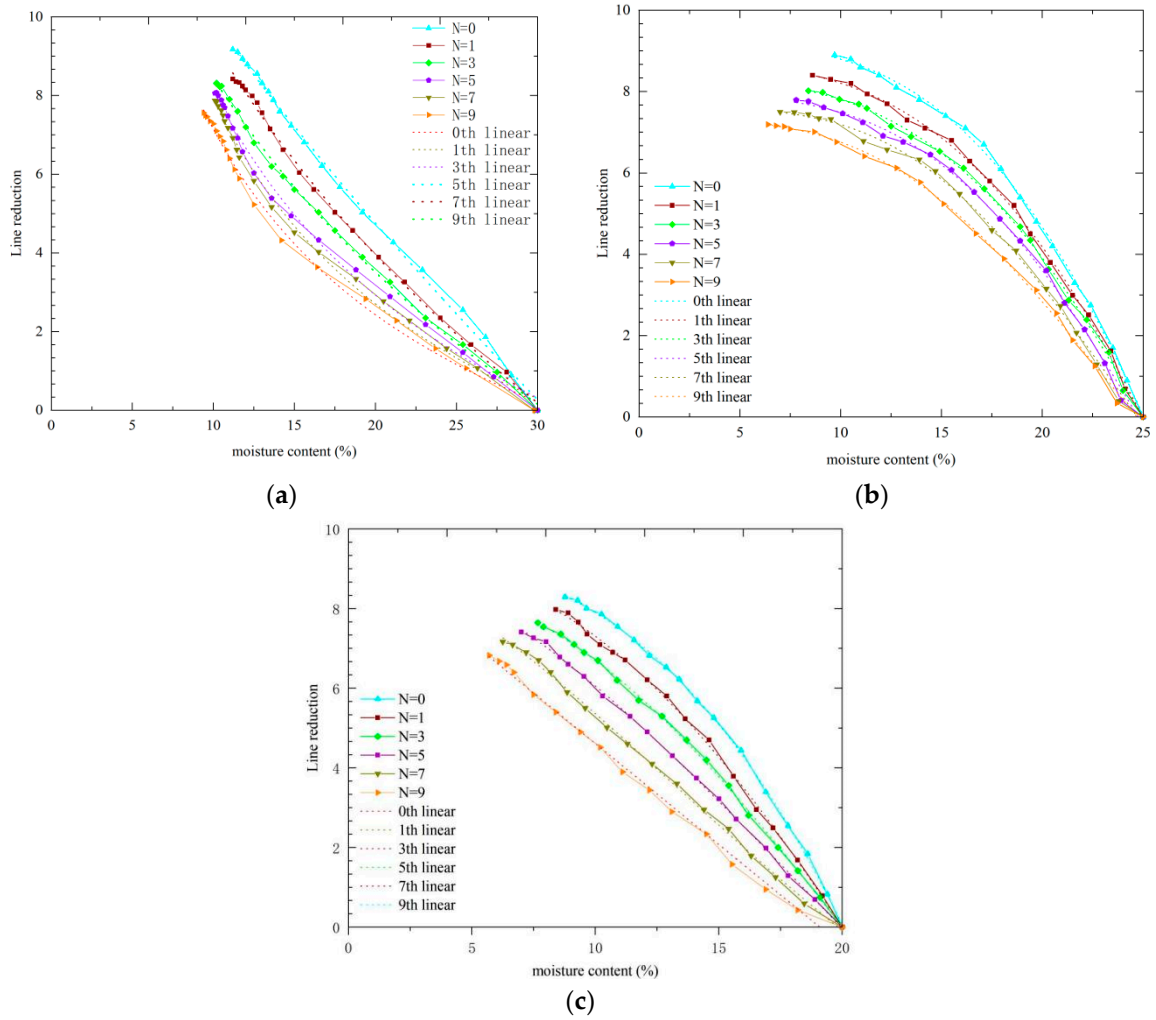

Figure 10. Linear fit of shrinkage curve with different number of cycles. (**a**) Fitted curves within the linear shrinkage phase of soil samples with an initial moisture content of 30% under different wet and dry cycling conditions; (**b**) fitted curves within the linear shrinkage phase of soil samples with an initial moisture content of 25% under different wet and dry cycling conditions; (**c**) fitted curves within the linear shrinkage phase of soil samples with an initial moisture content of 20% under different wet and dry cycling conditions.

Table 5. Fitted equations after different numbers of dry–wet cycles.

Initial Moisture Content 30%			
Cycle Times/Time	**Regression Equation**	**Correlation Coefficient**	**Corresponding Slope (β)**
0	$\varepsilon = -0.5007n + 0.1516$	0.9992	0.5007
1	$\varepsilon = -0.4425n + 0.1334$	0.9994	0.4425
3	$\varepsilon = -0.4146n + 0.1231$	0.9400	0.4146
5	$\varepsilon = -0.3887n + 0.1139$	0.9939	0.3887
7	$\varepsilon = -0.3638n + 0.1059$	0.9924	0.3638
9	$\varepsilon = -0.3535n + 0.1013$	0.9874	0.3535

Note: The formula δ is the line shrinkage rate, β is the shrinkage coefficient, n is the number of cycles.

Based on Figure 10 and Table 6, the axial shrinkage coefficient of the remodeled Yili loess decreases with increased wet and dry cycles. The relationship curve between the number of wet and dry cycles and the shrinking coefficient is reduced (see Figure 11). The shrinkage coefficient decreases as the number of cycles increases and shows a good exponential relation, and the descriptive equations are shown in Equations (10)–(12).

$$\beta = 0.4799e^{-0.039n} \quad (10)$$

$$\beta = 0.4581e^{-0.04n} \quad (11)$$

$$\beta = 0.4369e^{-0.039n} \quad (12)$$

Equations (10) through (12) are the equations for 30%, 25%, and 20% moisture content, respectively, where n is the number of wet and dry cycles and β is the shrinking coefficient. The correlation coefficients between the computed results and the experimental test results for water contents of 30%, 25%, and 20% are 0.963–0.968.

Table 6. Structure parameters of binarization treated loess samples in the study area after different dry–wet cycles.

Number of Wet and Dry Cycles (N)	Surface Crack Rate (%)	Surface Porosity (%)	Surface Area (cm)	Area of Contraction (mm)	Maximum Crack Length (mm)
0					
1	1.7	34.3	0.135	155.42	1.3517
3	2.3	27.1	0.084	122.62	1.7408
5	5.56	24.5	0.062	225.03	2.5421
7	5.95	24.9	0.054	320.63	3.6439
9	6.02	24.7	0.041	342.16	3.9489

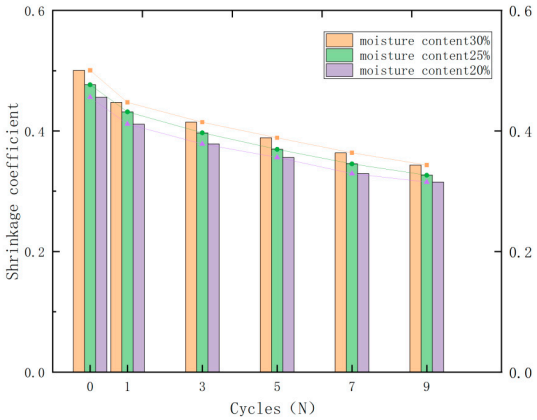

Figure 11. Relationship curve between the number of cycles and shrinkage coefficient.

3.5. Impact of Wet and Dry Cycles on the Rate of Fracture and the Rate of Shrinkage

The obtained images (see Figure 12) were processed using Image-Pro Plus 6.0 software, which can identify the particles, pores, and fissure systems in the images and automatically calculate basic geometric parameters such as their areas, perimeters, orientations, and shape coefficients. In order to characterize the fissure and shrinkage properties of loess during the shrinkage process, the microanalysis of the soil body should be focused on the following aspects: the surface fissure, the surface porosity, the surface area, shrinkage area, and fracture length in relation to multiple wet and dry cycles (see Table 6). The main operations are as follows:

(1) Click file-open to open an SEM image of clay.
(2) The "Segmentation" dialog box pops up. The program will automatically segment the image to obtain the binary slit image. Click "OK" to return.
(3) Click on "Auto analysis" to automatically remove stray dots, repair the rift, and bring up the rift network block information table.

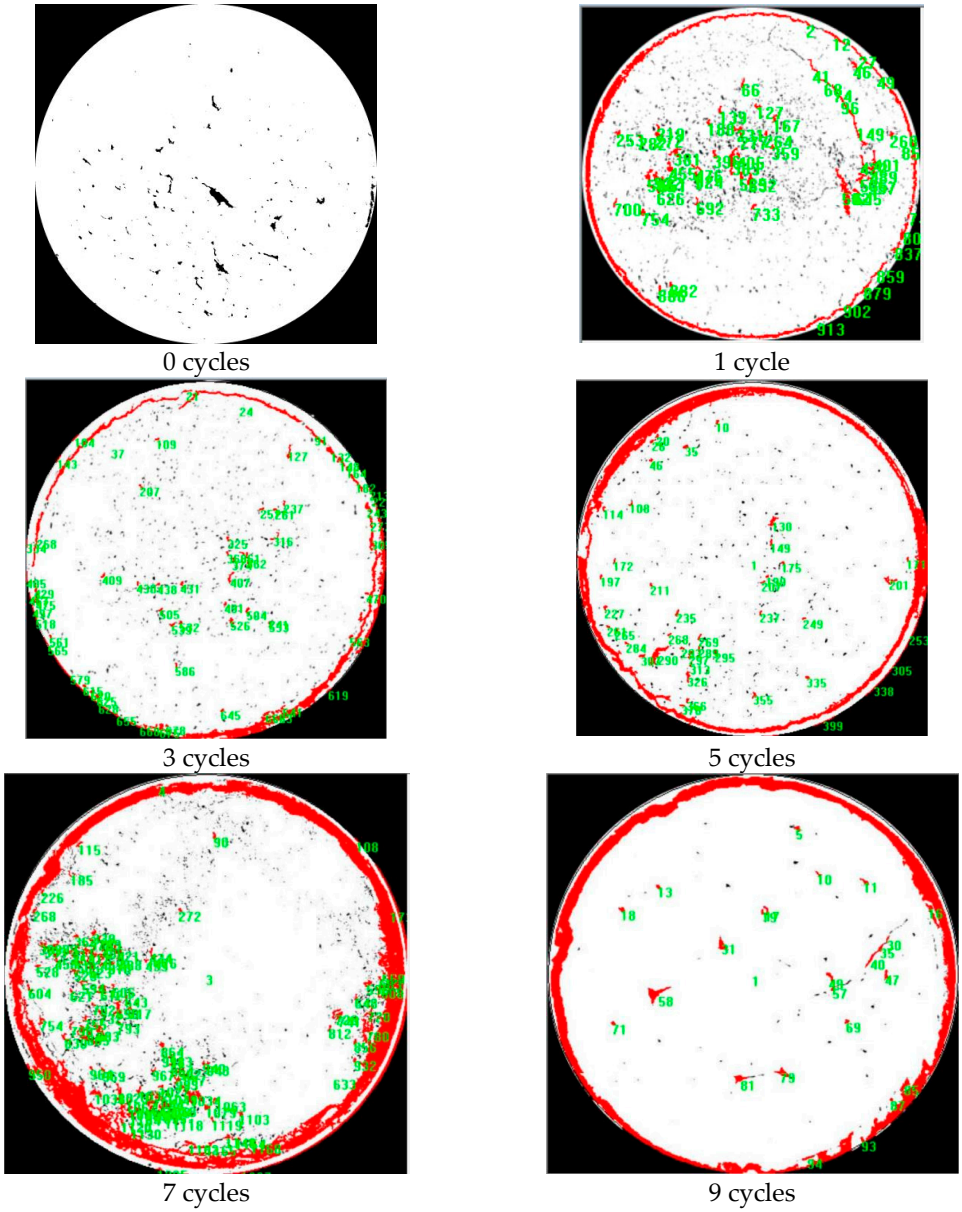

Figure 12. Specimen after binarization process. (The green data in the figure shows the area of the surface cracked area of the soil sample, and the red color shows the surface cracked area.)

Through software analysis, the following results were obtained. The deformation of the soil sample was affected by the number of dry and wet cycles. Small cracks appeared on the surface of the sample during the process of dry and wet cycles, and there was no change for zero cycles. During 1–5 cycles, the original cracks accumulated and expanded, the cracks of the sample repeatedly closed and opened, and the large cracks increased (as shown in Figure 13). With the increase in the number of cycles, the surface of the sample showed obvious expansion and deformation, and the surface porosity gradually increased. Subsequently, the pores of the sample reached a saturation state, and the change in porosity gradually stabilized after 5–6 cycles (as shown in Figure 14). In the dry–wet cycle, the sample volume shrinks in the first cycle, the content of fine particles in the soil sample decreases, and the surface area decreases. In the process of dehumidification, the surface dehydration rate of the soil sample is relatively fast. In the process of the 1st~3rd dry–wet cycle, the sample begins to show small cracks and gradually breaks away from the ring blade. The cracks extend to the center of the sample and continue to develop vertically until the 5th~7th dry–wet cycle. The original fissure accumulated and expanded, the damage degree of the sample further increased, the shrinkage was obvious, and the total deformation of the sample reached the maximum, being almost unchanged at the ninth dry–wet cycle (as shown in Figure 15). In the process of the dry and wet cycle, the shrinkage area of the sample increases first, then reaches the limit, and then gradually becomes stable. With the increase in initial water content, the initial axial shrinkage rate of all samples decreased, and the initial circumferential shrinkage rate increased. The loess body shrinkage rate kept increasing, but it did not change the shape of the shrinkage curve, while the size of large pores gradually decreased and the distribution density also decreased, resulting in changes in the soil structure, thus changing the shrinkage properties of the samples (as shown in Figure 16).

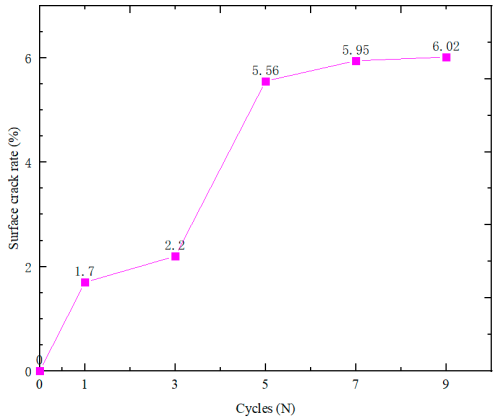

Figure 13. Surface cracking rate and number of cycles.

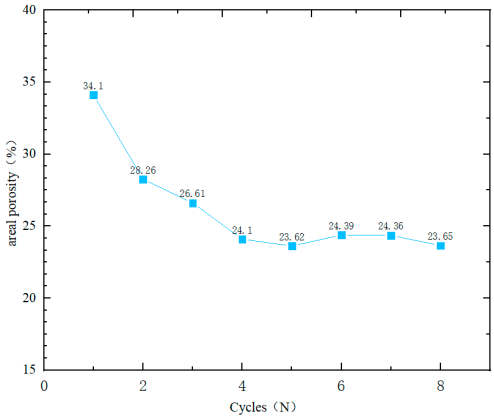

Figure 14. Surface porosity—number of cycles.

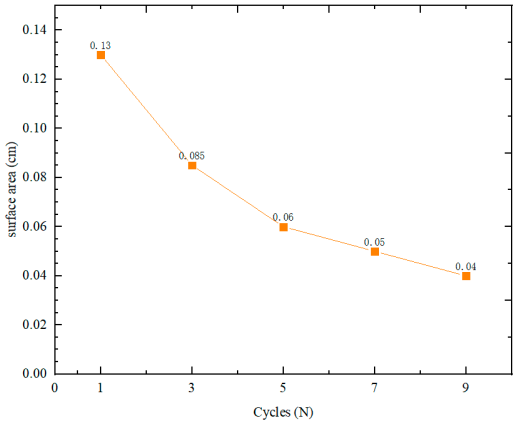

Figure 15. Surface area and number of cycles.

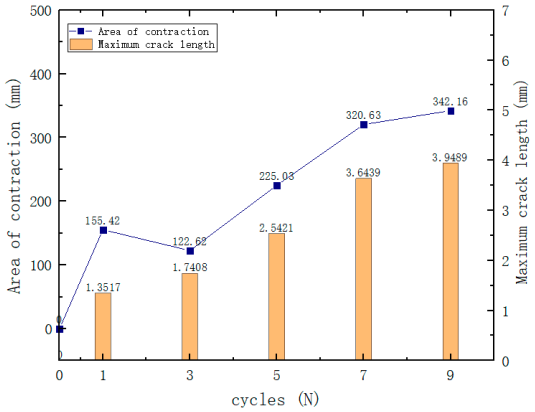

Figure 16. Shrinkage area, fracture length, and number of cycles.

4. Discussion

The effects of different moisture contents on loess are not completely the same, and the dry–wet cycle has a certain influence on the deterioration of loess. The shrinkage deformation characteristics and the change process of the microstructure of the remodeled Yili loess under the action of multiple dry–wet cycles were investigated. In this work, the law of shrinkage influence of loess under the condition of dry–wet cycle is basically consistent with the expectation and previous research results [9]. Before five dry–wet cycles, the edge of the sample gradually separated from the ring knife wall, and the cracks gradually contracted. The shrinkage change in loess was obvious, and the dry shrinkage cracks were superficial, thin in width, irregular in distribution, and uneven in distribution. With the change in surface humidity, surface shrinkage can cause cracks on the surface and inside the loess, ranging from small to large and gradually increasing in depth. The number of dry–wet cycles and the change in loess shrinkage are related to the change in soil water-holding capacity. In addition, the importance of shrinkage in the structure is mainly related to cracks. There are relatively few research results on the changes in the physical properties and microstructure of loess under the dry–wet cycle. In this study, the most relevant factors affecting the water-holding and shrinkage characteristics of the loess in Yili Valley of Xinjiang with different initial water contents and dry–wet effects were found, which can provide a reference for the prevention and control of geological disasters in the study area.

Wet–dry cycles include drying and humidification processes. During the drying process, the influence of the displacement constraint on the structure variation and shrinkage deformation of soil under small confining pressure gradually weakens with the increase in soil thickness (Zeng et al., 2019, Al-Jeznawi et al., 2021, Lin et al., 2021, Cuadrado et al., 2022) [46]. The results revealed that with the increase in dry–wet cycles, the mass loss of

soil deteriorated, and the surface crack rate increased. The cohesion of soil showed an overall decreasing trend, which decreased more obviously in the early stage of the dry–wet cycle, followed by a slow decrease, and tended to be constant after nine dry–wet cycles. However, the internal friction angle increased and then decreased during the whole cycle, and its value generally changed little.

The sample in this paper is remodeled loess from Yili Valley, and shrinkage experiments under different initial moisture content and dry–wet cycle conditions were carried out. In the future, the comparison between remodeled loess and original loess under different density conditions can be further considered, along with the change law of the mechanical properties of Yili loess and the remodeled loess. In addition, for the analysis of microstructure, more microstructure parameters should be further selected so as to explain the microscopic process of macroscopic mechanical property changes more comprehensively. This work relied on the loess landslide geological hazard survey and control project in this region and the National Natural Science Foundation of China (41967036).

5. Conclusions

In order to study the influence of dry and wet cycles on the water-holding properties of remodeled soil samples, and thus on loess landslides in the Yili Valley, the number of dry and wet cycles, the initial water content, and other test parameters were determined. Based on this, the laws of change in different initial water contents were established, and dry and wet conditions, linear shrinkage rate, shrinkage coefficient, final linear shrinkage rate, surface crack rate, and other characteristics were analyzed. The main conclusions are as follows:

(1) Based on the analysis, there is an exponential relationship between the number of wet and dry cycles and the final line shrinkage rate. The effect of wet and dry cycles on the final line shrinkage rate is more significant in the early stage, and the decrease in the final line shrinkage rate decreases as the number of wet and dry cycles increases.

(2) The dehumidification deformation of loess is divided into crack deformation and shrinkage deformation. In the qualitative assessment, cracks appeared at the edge of the sample after one to three cycles. After the fifth cycle, cracks and shrinkage deformation were evident. In the seventh cycle, the shrinkage deformation reached a stable state.

(3) Quantitative evaluation was conducted on the fracture area percentage and shrinkage area percentage of the loess. The sample underwent the plastic deformation stage in the first seven dry and wet cycles, and then gradually reached elastic deformation. In short, with the increase in the number of dry and wet cycles, the surface porosity gradually increases, and the dry and wet cycles make the pores shrink and expand. When the water is lost, the soil sample shrinks, but it cannot be recovered, and the pore area becomes larger and smaller. In the long-term dry–wet cycle, the pores of soil samples change, so the water-holding characteristics and strength characteristics of loess gradually deteriorate, and the dry–wet cycle leads to structural changes in soil mass.

(4) The microstructural changes in the shrinking basic structural units of loess described in this study explain the mechanical behavior of wet and dry cycling and how it affects the strength and basic structural units of loess, and the fitting relationship between wet and dry cycling and shrinkage properties is established. The macroscopic and microscopic analyses can provide technical support and theoretical references for the strength and microstructural deterioration effects of remodeled loess in the Ili River Valley. However, the relationships in this study still need to be analyzed and verified in more detail in future studies.

Author Contributions: Conceptualization, A.A. and W.C.; methodology, A.A.; software, W.C.; validation, A.A., Y.Z. and Z.Z.; formal analysis, A.A.; investigation, A.A.; resources, Z.Z.; data curation, A.A.; writing—original draft preparation, A.A.; writing—review and editing, A.A.; visualization, Z.Z.; supervision, Z.Z.; project administration, Z.Z.; funding acquisition, Z.Z. All authors have read and agreed to the published version of the manuscript.

Funding: This work relied on the loess landslide geological hazard survey and control project in this region and the National Natural Science Foundation of China (41967036).

Data Availability Statement: The data used to support the findings of this study are included in the manuscript.

Conflicts of Interest: The authors declare no conflict of interest.

References

1. Wang, X.M.; Mai, Z.J. Causal mechanism and deformation characteristics of typical mega loess landslide cluster in Yili, Xinjiang. *J. Water Resour. Archit. Eng.* **2016**, *4*, 195–200.
2. *GB50476-2008*; Code for Durability Design of Concrete Structures. China Architecture and Building Press: Beijing, China, 2008.
3. Hobbs, D.W.; Matthews, J.D.; Marsh, B.K. *Minimum Requirements of Durable Concrete: Carbonation and Chloride-Induced Corrosion, Freeze-Thaw Attack and Chemical Attack*; British Cement Association: Hertfordshire, UK, 1998.
4. McCarter, W.J.; Watson, W.D.; Chrisp, T.M. Surface zone concrete: Drying, absorption, and moisture distribution. *ASCE J. Mater. Civ. Eng.* **2001**, *13*, 49–57.
5. Tse, E.Y.M.; Ng, C.W.W. Effects of drying and wetting cycles on unsaturated shear strength. In Proceedings of the First European Conference on Unsaturated Soils, Durham, UK, 2–4 July 2008.
6. Ng, C.W.W.; Pang, Y.W. Experimental investigations of the soil-water characteristics of avolcanic soil. *Can. Geotech. J.* **2000**, *37*, 1252–1254. [CrossRef]
7. Kay, B.D.; Dexter, A.R. The influence of dispersible clay and wetting-drying cycles on thetensile strength of a red-brown earth. *Aust. J. Soil Res.* **1992**, *30*, 297–310. [CrossRef]
8. Malusis, M.A.; Yeom, S.; Evans, J.C. Hydraulic conductivity of model soil–bentonite backfills subjected to wet-dry cycling. *Can. Geotech. J.* **2011**, *48*, 1198–1211. [CrossRef]
9. Mao, Y.C.; Li, G.Y.; Lei, J.X.; Zhang, L.R.; Chen, Z.Y. Experimental study on the effects of wetting-drying cycles of compacted loess. *Adv. Mater. Res.* **2014**, *831*, 326–330. [CrossRef]
10. Yuan, H. Indoor Test of Collapsibility of Loess and Microstructure Research. Master's Thesis, Taiyuan University of Technology, Taiyuan, China, 2008.
11. Shao, S.J.; Luo, A.Z.G.; Zhou, F.F. Structural damage characteristics of Q3 clay loess under loading and humidification. *Chin. J. Geotech. Eng.* **2006**, *28*, 2077–2081.
12. Zhang, F.Z.; Chen, X.P. Effects of repeated wetting and drying cycles on mechanical properties of unsaturated soils. *Chin. J. Geotech. Eng.* **2010**, *32*, 41–46.
13. Luan, M.T.; Wang, D.L.; Yang, Q. Experimental study on drying shrinkage of unsaturated remolded soils. *Chin. J. Geotech. Eng.* **2008**, *30*, 118–122.
14. Wang, D.L. Experimental study on saturation and porosity ratio of remolded soil in drying process. *Geotech. Eng.* **2008**, *11*, 27–28.
15. Pires, L.F.; Bacchioos, R. Gamma ray computed tomography to evaluate wetting/drying soil structure changes. *Nucl. Instrum. Methods Phys. Res. B* **2005**, *229*, 443–456. [CrossRef]
16. Pires, L.F.; Cooper, M.; Cassaro, F.A.M.; Reichardt, K.; Bacchi, O.O.S.; Dias, N.M.P. Micromorphological analysis to characterize structure modifications of soil samples submitted to wetting and drying cycles. *Catena* **2008**, *72*, 297–304. [CrossRef]
17. Liu, P. Research on the Mechanism of Surface Drying and Cracking of Earthen Architectural Sites. Doctoral Dissertation, Lanzhou University, Lanzhou, China, 2009.
18. Wang, D.L. In the process of drying remolded soil saturation and porosity ratio experimental study. *Geotech. Eng.* **2008**, *8*, 27–28.
19. Wang, D.L. Experimental Study on Unsaturated Soil and Its Application to Land Subsidence. Ph.D. Thesis, Dalian University of Technology, Dalian, China, 2007. (In Chinese)
20. Hui, T.; Li, L.I.; Kun, Z.; Peng, W. Effects of dry, wet and freeze-thaw cycles on the microstructure of Loess. *J. Lanzhou Univ. Technol.* **2020**, *46*, 122–127.
21. Ye, W.M.; Wan, M.; Bao, C. Microstructure characteristics of high pressure bentonite under dry and wet cycle. *Chin. J. Geotech. Eng.* **2020**, *33*, 1173–1177.
22. Wu, Y.X. *Quantitative Study on Microstructure of Engineering Clay*; Graduate Department of Chinese Academy of Geological Sciences: Beijing, China, 1991; pp. 143–151. (In Chinese)
23. Wang, B.J.; Bin, S.H.I. 3D visualization and porosity calculation of SEM images of clay soil based on GIS. *Rock Soil Mech.* **2008**, *29*, 251–255.
24. Shi, B.; Li, S.L. Quantitative study on microstructure of clay by SEM image. *Sci. China* **1995**, *25*, 666–672.
25. Shi, B. Quantitative study on the orientation of clay microstructure. *Acta Geol. Sin.* **1997**, *71*, 36–44.

26. Shi, B. Review and Prospect of clay microstructure research. *J. Eng. Geol.* **1996**, *4*, 39–44.
27. Shi, B. Simple quantitative analysis of clay microstructure. *Hydrogeol. Eng. Geol.* **1997**, *1*, 7–10. [CrossRef]
28. Collins, K.; McGown, A. The form and function of microfabric features in a variety of natural soils. *Geotechnique* **1974**, *24*, 223–254.
29. Yong, R.N.; Warkentin, B.P. *Soil Properties and Behavior*; Megill University: Montreal, QC, Canada, 1975.
30. Hu, C.M.; Yuan, Y.L.; Wang, X.Y.; Mei, Y.; Liu, Z. Experimental Study on Strength Deterioration Model of Compacted Loess under Wetting-drying Cycles. *Chin. J. Rock Mech. Eng.* **2018**, *37*, 2804–2818.
31. Wanjun, Y.E.; Changqing, L.I.; Gengshe, Y.; Xiao, L.I.; Hui, L.I. Evolution of Loess Crack under Action of Dehumidification-Humidification. *J. Eng. Geol.* **2017**, *25*, 376–383.
32. Wang, T.H.; Hao, Y.Z.; Wang, Z.; Cheng, L.; Li, J. Experimental Study on Dynamic Strength Properties of Compacted Loess under Wetting-drying Cycles. *Chin. J. Rock Mech. Eng.* **2020**, *39*, 1242–1251.
33. Gallipoli, D.; Wheeler, S.J.; Karstunen, M. Modelling of variation of degree of saturation in a deformable unsaturated soil. *Géotechnique* **2003**, *53*, 105–112. [CrossRef]
34. Metelková, Z.; Boháč, J.; Přikryl, R.; Sedlářová, I. Maturation of loess treated with variable lime admixture: Pore space textural evolution and related phase changes. *Appl. Clay Sci.* **2012**, *61*, 37–43.
35. Mu, Y.-H.; Ma, W.; Li, G.-Y.; Mao, Y.-C. Quantitative analysis of impacts of freeze–thaw cycles upon microstructure of compacted loess. *Chin. J. Geotech. Eng.* **2011**, *33*, 1919–1925.
36. Tang, C.S.; Shi, B.; Liu, C.; Zhao, L.; Wang, B. Influencing factors of geometrical structure of surface shrinkage cracks in clayey soils. *Eng. Geol.* **2008**, *101*, 204–217. [CrossRef]
37. Tang, C.S.; Cui, Y.J.; Tang, A.M.; Shi, B. Experiment evidence on the temperature dependence of desiccation cracking behavior of clayey soils. *Eng. Geol.* **2010**, *114*, 261–266. [CrossRef]
38. Tang, C.S.; Shi, B.; Gu, K. Experimental investigation on evaporation process of water in soil during drying. *Chin. J. Eng. Geol.* **2011**, *19*, 875–881.
39. Vogel, H.J.; Hoffmann, H.; Roth, K. Studies of crack dynamics in clay soil: I. experimental methods, results, and morphological quantification. *Geoderma* **2005**, *125*, 203–211.
40. Güllü, H.; Agha, A.A. The rheological, fresh and strength effects of cold-bonded geopolymer made with metakaolin and slag for grouting. *Constr. Build. Mater.* **2021**, *274*, 122091. [CrossRef]
41. Güllü, H.; Al Nuaimi, M.M.D.; Aytek, A. Rheological and strength performances of cold-bonded geopolymer made from limestone dust and bottom ash for grouting and deep mixing. *Bull. Eng. Geol. Environ.* **2021**, *80*, 1103–1123. [CrossRef]
42. Güllü, H.; Fedakar, H.I. On the prediction of unconfined compressive strength of silty soil stabilized with bottom ash, jute and steel fibers via artificial intelligence. *Geomech. Eng.* **2017**, *12*, 441–464. [CrossRef]
43. Zhou, L.N. Experimental Study and Numerical Analysis of Water Loss Shrinkage of Loess. Master's Thesis, Xi'an University of Architecture and Technology, Xi'an, China, 2014. (In Chinese)
44. *JTG 3430-2020*; Test Methods of Soils for Highway Engineering. Ministry of Transport of the People's Republic of China: Beijing, China, 2021.
45. Tang, Q.; Liu, C.; Gu, Y.F.; Shi, B. Identification and statistical methods of soil microstructure in SEM images. *J. Guilin Univ. Technol.* **2017**, *37*, 547–552.
46. Zeng, H.; Tang, C.-S.; Cheng, Q.; Inyang, H.I.; Rong, D.-Z.; Lin, L.; Shi, B. Coupling effects of interfacial friction and layer thickness on soil desiccation cracking behavior. *Eng. Geol.* **2019**, *260*, 105220. [CrossRef]